The Journal of Chemical Physics

Modulating optical properties and interfacial electron transfer of $CsPbBr_3$ perovskite nanocrystals via indium ion and chlorine ion co-doping

Cite as: J. Chem. Phys. **155**, 234701 (2021); https://doi.org/10.1063/5.0076037
Submitted: 20 October 2021 • Accepted: 23 November 2021 • Accepted Manuscript Online: 23 November 2021 • Published Online: 15 December 2021

Jianfei Cao, Zuodong Yin, Qi Pang, et al.

The Journal of Chemical Physics ARTICLE scitation.org/journal/jcp

Modulating optical properties and interfacial electron transfer of $CsPbBr_3$ perovskite nanocrystals via indium ion and chlorine ion co-doping

Cite as: J. Chem. Phys. 155, 234701 (2021); doi: 10.1063/5.0076037
Submitted: 20 October 2021 • Accepted: 23 November 2021 •
Published Online: 15 December 2021

Jianfei Cao,[1] Zuodong Yin,[1] Qi Pang,[1,a)] Yuexi Lu,[1] Xiuqing Nong,[1] and Jin Zhong Zhang[2,a)]

AFFILIATIONS

[1] School of Chemistry and Chemical Engineering, Guangxi University, Nanning 530004, Guangxi, People's Republic of China
[2] Department of Chemistry and Biochemistry, University of California, Santa Cruz, California 95064, USA

Note: This paper is part of the JCP Special Topic on Transport of Charge and Energy in Low-Dimensional Materials.
[a)]**Authors to whom correspondence should be addressed:** pqigx@163.com and zhang@ucsc.edu

ABSTRACT

In this work, we demonstrated an *in situ* approach for doping $CsPbBr_3$ nanocrystals (NCs) with In^{3+} and Cl^- with a ligand-assisted precipitation method at room temperature. The In^{3+} and Cl^- co-doped NCs are characterized by the powder x-ray diffraction patterns, ultraviolet–visible, photoluminescence (PL) spectroscopy, time-resolved PL (TRPL), ultraviolet photoelectron spectroscopy, x-ray photoelectron spectroscopy, and transmission electron microscopy. Based on PL and TRPL results, the non-radiative nature of In^{3+}-doping induced localized impurity states is revealed. Furthermore, the impact of In^{3+} and Cl^- doping on charge transfer (CT) from the NCs to molecular acceptors was investigated and the results indicate that the CT at the interface of NCs can be tuned and promoted by In^{3+} and Cl^- co-doping. This enhanced CT is attributed to the enlarged energy difference between relevant states of the molecular acceptor and the NCs by In^{3+} and Cl^- upon co-doping. This work provides insight into how to control interfacial CT in perovskite NCs, which is important for optoelectronic applications.

I. INTRODUCTION

Recently, all-inorganic cesium lead halide ($CsPbX_3$, X = Cl, Br, I) perovskite (PVK) nanocrystals (NCs) have attracted enormous attention owing to their excellent optoelectronic properties.[1–3] In particular, the halide in $CsPbX_3$ NCs can be easily post-synthetically tailored through anion exchange with preserved size and shape.[4] By tuning the amount of different halogens, the electronic band structures and charge transfer (CT) properties of the NCs can be easily modulated.[5,6] For instance, Guo *et al.* adopted a mixed halide strategy and synthesized $CsPb(Br_x/Cl_{3-x})_3$ with enhanced activity toward CO_2 reduction while maintaining high selectivity of CO and CH_4 production.[7] Li *et al.* constructed perovskite solar cells based on a laminar $MAPbBr_3/MAPbBr_{3-x}I_x$ ($MA = CH_3NH_3^+$) graded heterojunction single crystal with high external quantum efficiency (EQE) and short response time, attributed to improved carrier extraction and suppressed recombination loss.[8] Guan *et al.* found that $MAPbBr_{3-x}I_x$ exhibited excellent hydrogen production performance due to its bandgap funnel structure, which facilitated the photogenerated carrier transfer from the interior to the surface.[9] Since the anion exchange reaction starts from the surface of $CsPb(Cl/Br)_3$ or $CsPb(Br/I)_3$ particles, the concentration of Br^- or I^- on the surface is higher than that on the inside, which leads to a narrower bandgap at the surface and is favorable for efficient migration of carriers from the interior to the surface.[10]

Element doping has been demonstrated as one effective approach to modulating the foundational properties of the $CsPbBr_3$ perovskite without altering the original structure of the host crystal.[11–13] Heterovalent doping in semiconductors can change the charge carriers from *n*-type to *p*-type and vice versa.[14–16] Indium ion has been regarded as an appealing dopant to substitute Pb^{2+} in perovskites due to its low toxicity and the similar electron structure

with the Pb element.[17] In^{3+} doping of photocatalytic semiconductor materials can improve photogenerated carrier separation and promote photocatalytic activity.[18,19] Li *et al.* synthesized In-doped carbon nitride (In: CN) with higher CT efficiency and photocatalytic performance in H_2 generation.[20] Either smaller B- or X-site substitution ions were able to improve the efficiency of the photogenerated carrier separation.[20] Therefore, doping with In^{3+} smaller than Pb^{2+}, Cl^- smaller than $Br^-$is expected to have a synergy effect to facilitating the CT and carrier separation of $CsPbBr_3$.

Herein, we demonstrate an In^{3+} and Cl^- co-doping strategy by incorporating indium chloride ($InCl_3$) into $CsPbBr_3$ NCs and investigate the effect of cation and anion co-exchange on CT of the $CsPbBr_3$ perovskite. The In^{3+} doped $CsPb(Br/Cl)_3$ NCs were obtained using the ligand-assisted precipitation method in one step at room temperature under ambient conditions. The exchange between In^{3+} and Pb^{2+} introduces more defect states that provide alternative pathways for electron relaxation.[21,22] The photoluminescence (PL) of $CsPbBr_3$ NCs is quenched with increasing concentrations of $InCl_3$, indicating increased non-radiative recombination of carriers.[23] PL and time-resolved PL (TRPL) results reveal the influence of doping on the energy bandgap and PL quenching of $CsPbBr_3$ NCs with tetracyanoethylene (TCNE) as an electron acceptor. This study shows that In^{3+} and Cl^- co-doping plays a key role in regulating the CT behavior to achieve high charge separation efficiency, with potential applications in optoelectronics.

II. EXPERIMENTAL SECTION

A. Chemicals

Oleic acid (OA, 99%, Aladdin), oleylamine (Oam, 99%, Aladdin), cesium bromide (CsBr, 99.9%, Aladdin), lead bromide ($PbBr_2$, 99.999%, Aladdin), cesium chloride (CsCl, 99.9%, Aladdin), lead chloride ($PbCl_2$, 99.9%, Aladdin), indium (III) chloride ($InCl_3$, 99%, Aladdin), indium (III) bromide ($InBr_3$, 99.9%, Macklin), tetracyanoethylene (TCNE, 99%, Aladdin), *N*,*N*-dimethylformamide (DMF, 99.5%, Macklin), dimethyl sulfoxide (DMSO, 99.5%, Macklin), and toluene (99.5%, Chron Chemical) were used as purchased without any further purification.

B. Synthesis of $CsPbBr_3$ NCs

$CsPbBr_3$ was synthesized using the ligand-assisted precipitation method under ambient conditions with some modifications. Typically, CsBr (0.040 mmol) and $PbBr_2$ (0.040 mmol) were dissolved in DMF (1.0 ml), and 0.15 ml oleic acid (OA) and 0.050 ml oleylamine (Oam) were added when the solution was stirred to be transparent. Then, the precursor was swiftly injected into 10 ml toluene under vigorous stirring to obtain the $CsPbBr_3$ NCs.

C. Synthesis of In^{3+} doped $CsPb(Br/Cl)_3$ NCs

The synthesis of In^{3+} doped $CsPb(Br/Cl)_3$ NCs was similar as $CsPbBr_3$ with some modifications. Taking the In/Pb molar ratio of 0.5 as an example, 8.5 mg CsBr (0.040 mmol), 14.7 mg $PbBr_2$ (0.040 mmol), and 4.4 mg $InCl_3$ (0.020 mmol) were dissolved in DMF (1.0 ml), and then 0.15 ml OA and 0.050 ml Oam were added to form a precursor solution. Then, the precursor solution was quickly injected into 10 ml vigorously stirred toluene solution to obtain the In^{3+} doped $CsPb(Br/Cl)_3$ NCs. Another concentration of the In^{3+} doped $CsPb(Br/Cl)_3$ sample was synthesized by similar methods, and the amount of $InCl_3$ was 0.080 mmol, denoted as In/Pb 2. The as-synthesized In^{3+} doped $CsPb(Br/Cl)_3$ NCs were centrifuged at 4000 rpm for 5 min, and the supernatant was discarded. The precipitates were re-dispersed in toluene, washed twice, and centrifuged again at 4000 rpm for 5 min. The precipitate was collected, and the $CsPbBr_3$ perovskite powders were recovered by vacuum drying at 25 °C for 24 h. For the sake of comparison, the In^{3+} doped $CsPbBr_3$ NCs using $InBr_3$ as addition were prepared with the same method except $InCl_3$ was replaced by $InBr_3$. For the synthesis of $CsPbCl_3$, CsCl (0.040 mmol) and $PbCl_2$ (0.040 mmol) were dissolved in DMSO (1 ml), and 0.15 ml oleic acid (OA) and 0.050 ml oleylamine (Oam) were added when the solution was stirred to be transparent. Then, the precursor was swiftly injected into 10 ml toluene under vigorous stirring to obtain the $CsPbCl_3$ NCs. As for the preparation of NCs-TCNE mixtures, 0–10 μmol TCNE was added into 10 ml toluene solutions of NCs. The mixtures were sonicated for 10 min before optical measurements.

D. Characterizations

Ultraviolet–visible (UV–vis) electronic absorption and PL spectra were carried out using a UV-5500PC spectrometer (METASH, China) and a FLS-1000 fluorescence spectrometer (Edinburgh Instruments, UK), respectively, in a quartz cuvette at room temperature. X-ray diffraction (XRD) analysis was performed on a SMARTLAB diffractometer using Cu Kα radiation at a voltage of 40 kV and a current of 30 mA to explore the crystalline phase. The x-ray photoelectron spectroscopy (XPS) and ultraviolet photoemission spectroscopy (UPS) measurements were carried out using a Thermo Fisher Scientific Escalab 250Xi spectrometer. The excitation source for XPS measurements was a monochromatic Al-Kα x-ray source (1486.6 eV) to identify the chemical composition. The UPS measurements were carried out with a 21.2 eV He-Iα source and a −10 eV bias. The samples for UPS were prepared by casting NCs on a 5 × 5 mm^2 FTO substrate. Element content analysis was performed using an Agilent 720 inductively coupled plasma-optical emission spectrometer (ICP-OES). The absolute photoluminescence quantum yield (PLQY) measurements were recorded using an Edinburgh Instruments integrating sphere with a FLS-1000 fluorescence spectrometer and PMT-900 detector. The high-resolution transmission electron microscopy (HRTEM) images and energy dispersive x-ray (EDX) were determined using a transmission electron microscope (FEI TECNAI G2 F30) operating at an acceleration voltage of 300 kV. The time correlated single photo counting (TCSPC) was employed using the EPL-TCSPC system and PMT-900 detector for time-resolved luminescence measurements.

III. RESULTS AND DISCUSSION

$CsPbBr_3$ perovskite NCs capped with OA and Oam were synthesized using the ligand-assisted reprecipitation method, as illustrated in Fig. 1. The crystal structure of $CsPb(Br/Cl)_3$ NCs is a cubic perovskite structure, and their space group is Pm-3m upon introducing In^{3+}; some Pb^{2+} ions were substituted by In^{3+} to form a $[In(Cl/Br)_6]^{3-}$ octahedron.

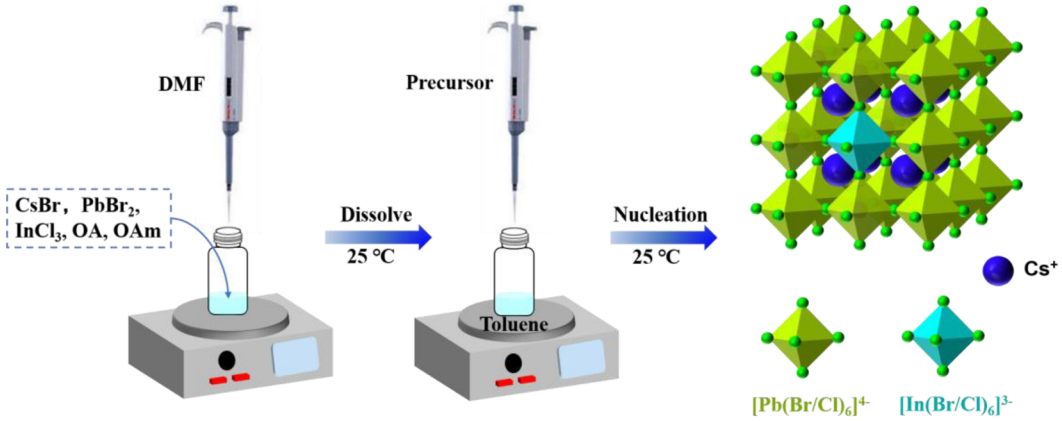

FIG. 1. Schematic illustration of the formation of the In^{3+} doped $CsPb(Br/Cl)_3$ NCs.

The XRD spectra of doped and undoped $CsPbBr_3$ NCs are shown in Fig. 2(a). All peaks of three samples match well with the cubic phase structure of $CsPbBr_3$ (No. 54-0752) with no impurity phase, which is consistent with previous report.[24] The diffraction peaks at 15.15°, 21.55°, 30.64°, 34.58, 37.76°, and 43.89° are assigned to (100), (110), (200), (210), (211), and (220) planes, respectively. For In^{3+} doped $CsPbBr_3$ NCs, all peaks slightly shifted to higher angles, which is consistent with the lattice contraction caused by the substitution of Pb^{2+} (119 pm) by In^{3+} (80 pm), which indicated that In^{3+} could be introduced in the $CsPbBr_3$ lattice. For In^{3+} doped $CsPb(Br/Cl)_3$ NCs, the peaks distinctly shift to higher angles compared to pristine $CsPbBr_3$ [Fig. 2(b)] due to the lattice contraction caused by the substitution of Pb^{2+} by In^{3+} and Br^- (196 pm) by Cl^- (181 pm).[25]

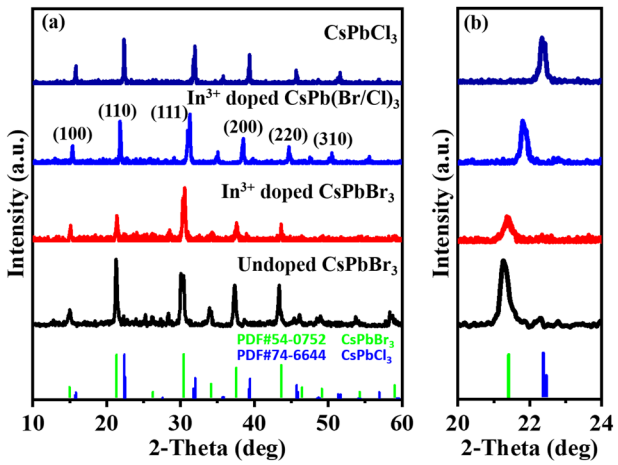

FIG. 2. (a) XRD patterns of undoped $CsPbBr_3$ NCs, In^{3+} doped $CsPbBr_3$ NCs, and In^{3+} doped $CsPb(Br/Cl)_3$ NCs (In/Pb 0.5). (b) Magnification of the XRD patterns in the 20°–24° range.

TEM and HRTEM images reveal the morphology and size of the undoped and In^{3+} doped $CsPb(Br/Cl)_3$ NCs. Both samples show a cubic shape, and the average dimensions of the undoped $CsPbBr_3$ NCs are ~16.54 and 13.15 nm for long and short edges [Figs. S1(a)–S1(d)], while those of the In^{3+} doped $CsPb(Br/Cl)_3$ NCs are 9.40 and 8.21 nm, respectively [Figs. 3(a)–3(d)]. The interplanar spacing of In^{3+} doped $CsPb(Br/Cl)_3$ NCs is 0.41 nm, which corresponds to the (110) crystal plane from HRTEM. The energy dispersive x-ray (EDX) spectra (Fig. S2) and mapping images [Figs. 3(e)–3(i)] clearly showed the relative peak intensity and element distribution including Cs (21.09%), Pb (18.75%), Br (42.53%), In (0.78%), and Cl (16.84%), which demonstrated that In^{3+} and Cl^- were incorporated into the perovskite lattice in low concentrations. In the In/Pb 0.5 sample, the actual doping level of In^{3+} was estimated to be 2.23% by inductively coupled plasma-optical emission spectrometry (ICP-OES).

To further confirm that In^{3+} and Cl^- were successfully incorporated into $CsPbBr_3$ NCs, x-ray photoelectron spectroscopy (XPS) was conducted to investigate the surface chemical environment of In^{3+} doped $CsPb(Br/Cl)_3$ NCs in comparison to that of undoped $CsPbBr_3$ NCs. As shown in Fig. 4(a), both doped (In/Pb 0.5) and undoped $CsPbBr_3$ NCs exhibit distinct peaks correlated with Cs, Pb, Br, C, and O elements. High-resolution spectra show the core-level peaks of Cs 3d (Cs $3d_{3/2}$: 738.1 eV and Cs $3d_{5/2}$: 724.2 eV), Pb 4f ($4f_{5/2}$: 143.0 eV and $4f_{7/2}$: 138.2 eV), and Br 3d ($3d_{3/2}$: 68.9 eV and $3d_{5/2}$: 68.0 eV) for In^{3+} doped $CsPb(Br/Cl)_3$ NCs. All the binding energy was slightly higher compared to the pristine $CsPbBr_3$ NCs due to the alternant chemical environment of the $[PbBr_6]^{4-}$octahedron and the enhancement of the interaction between Pb–Br and Cs–Br upon In^{3+} and Cl^- doping.[17,26] Meanwhile, the binding energies of In 3d peaks were 452.6 and 445.1 eV, corresponding to In $3d_{3/2}$ and $3d_{5/2}$, respectively. The Cl 2p peaks at 199.3 and 197.6 eV correspond to Cl $2p_{1/2}$ and $2p_{3/2}$, indicating the existence of In^{3+} and Cl^- in $CsPbBr_3$ NCs [Figs. 4(b)–4(f)].[25] The atomic proportion of In/Cs/Pb/Br/Cl in the In^{3+} doped $CsPb(Br/Cl)_3$ NCs surveyed from the XPS spectra is 3.39/16.16/11.23/45.07/24.35, respectively, consistent with the result of ICP-OES.

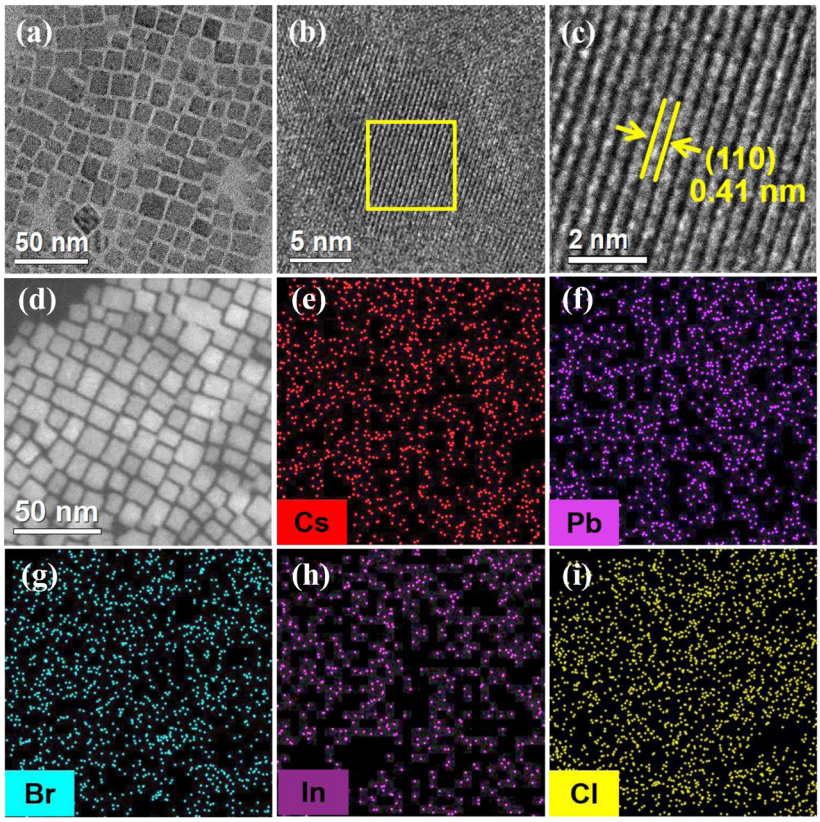

FIG. 3. (a)–(d) TEM and HRTEM images of In^{3+} doped $CsPb(Br/Cl)_3$ NCs. (e)–(i) Elemental mappings of Cs, Pb, In, Br, and Cl in In^{3+} doped $CsPb(Br/Cl)_3$ NCs.

Figure 5(a) shows the UV–vis electronic absorption spectra of undoped and In^{3+} doped NCs. The undoped NCs exhibit a sharp first excitonic absorption feature around 516 nm, while the In^{3+} doped $CsPbBr_3$ NCs have absorption around 523 nm.[27] With In^{3+} and Cl^- co-doping, the resulting NCs exhibit the first excitonic absorption peak around 462 nm due to Cl^- substituting parts of Br^-.[28] The results indicate successful doping of In^{3+} and Cl^- into the $CsPbBr_3$ NCs. The optical bandgap (E_{opt}) of the In^{3+} doped $CsPb(Br/Cl)_3$ NCs estimated from the UV–vis absorption spectra is 2.68 eV. The presence of Urbach tailing in the doped NCs suggests that there was lattice distortion upon doping.[29] The narrow excitonic bands of the doped NCs indicate uniform particle size distribution.

Under excitation at 365 nm, the PL emission peak of undoped $CsPbBr_3$ is 519 nm with a Stokes shift of 9 nm [Figs. 5(a) and 5(b)]. For In^{3+} doped $CsPbBr_3$ NCs, the PL emission peak slightly shifts to longer wavelength to 535 nm with lower intensity compared with the undoped $CsPbBr_3$ NCs [Figs. 5(a) and 5(b)]. This result suggests that In^{3+} leads to PL quenching, possibly due to bandgap trap states introduced.[19] For the In^{3+} doped $CsPb(Br/Cl)_3$ NCs, the sample (In/Pb 0.5) exhibits a maximum emission wavelength at 461 nm with a narrow full width at half-maximum (FWHM) of about 21 nm [Fig. 5(b)]. With increasing amount of $InCl_3$, the emission peak shifted to 425 nm, which is attributed to the larger bandgap of Cl-rich $CsPb(Br/Cl)_3$.[30,31] At the same time, the PL intensity substantially decreased with increasing doping level. Such a significant decrease in PL intensity suggests that In^{3+} and Cl^- be incorporated into the $CsPbBr_3$ host lattice and introduce bandgap trap states.[15,19,32]

TRPL was measured to help understand the effect of doping on carrier lifetime and PL quenching mechanisms. As shown in Fig. 6, the PL decay profiles of all the samples were both well-fitted with a biexponential function,

$$I(t) = A_1 e^{-t/\tau_1} + A_2 e^{-t/\tau_2}, \quad (1)$$

where A_1 and A_2 are amplitudes and τ_1 and τ_2 are the fast and slow decay components, respectively. The average lifetimes were calculated using the following equation:

$$\tau_{ave} = (A_1\tau_1^2 + A_2\tau_2^2)/(A_1\tau_1 + A_2\tau_2). \quad (2)$$

The TRPL data for the average lifetime of undoped and In^{3+} doped NCs are listed in Table S1. The average lifetime decreased from 16.06 to 14.27 ns and 9.29 ns for undoped $CsPbBr_3$ NCs, In^{3+} doped $CsPbBr_3$ NCs, and In^{3+} doped $CsPb(Br/Cl)_3$ NCs, respectively. For the In^{3+} doped $CsPb(Br/Cl)_3$ NCs, the lifetime for different doping amounts gradually decreased from 9.29 to 4.19 ns with increasing

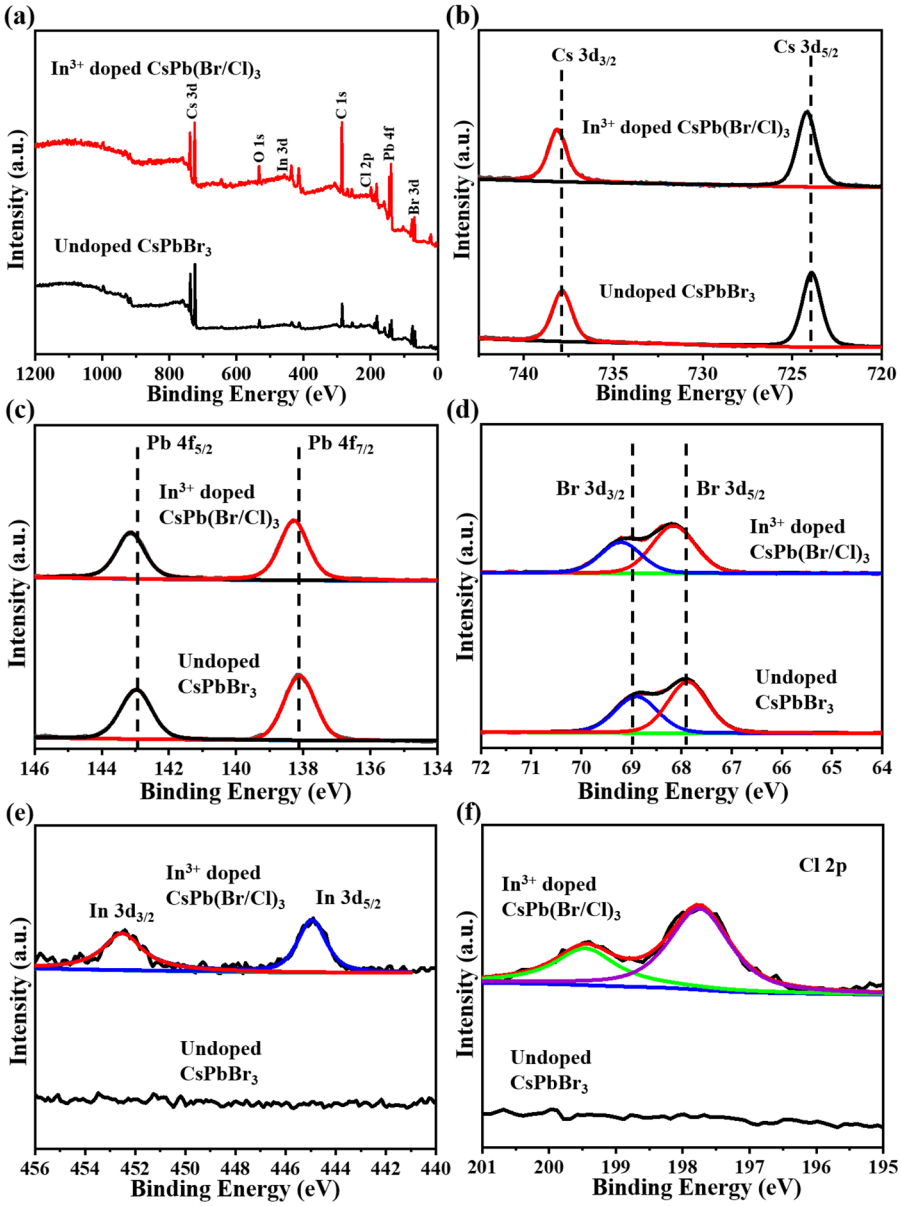

FIG. 4. XPS data corresponding to In^{3+} doped $CsPb(Br/Cl)_3$ NCs (a). Survey full scan and high-resolution XPS analysis of (b) Cs 3d, (c) Pb 4f, (d) Br 3d, (e) In 3d, and (f) Cl 2p. The high-resolution spectra were also recorded corresponding to the core levels of Cs 3d, Pb 4f, and Br 3d for the undoped NCs.

concentration of $InCl_3$ (Table S2). We can calculate the radiative (τ_r) and non-radiative lifetime (τ_{nr}) using the relationships between the average observed lifetime (τ_{obs}) and the measured PLQY,

$$\text{PLQY} = \tau_{obs}/\tau_r, \tag{3}$$

$$1/\tau_{obs} = 1/\tau_r + 1/\tau_{nr}. \tag{4}$$

The calculated values for τ_r and τ_{nr} are summarized in Table I. With increasing $InCl_3$, the radiative lifetime was longer, while the non-radiative lifetime was shorter, leading to the decreased PLQY. This result suggested that doping of $InCl_3$ could affect both radiative and non-radiative lifetimes.[33] It should be emphasized that Eqs. (3) and (4) are strictly valid only for single exponential PL decays. Therefore, the values obtained from these equations are approximations in this work. The PL quenching accompanied by a decrease in the PL decay lifetime in In^{3+} and Cl^- doped $CsPbBr_3$ NCs suggests the presence of trap states in the bandgap of the host $CsPbBr_3$ NCs upon doping with In^{3+} and Cl^-.[34] Such trap states provide alternative pathways for non-radiative electronic relaxation and consequently reduce radiative recombination.[15,35] In radiative and the calculated results of radiative and non-radiative lifetimes indicate that the radiative lifetime increased and non-radiative lifetime significantly

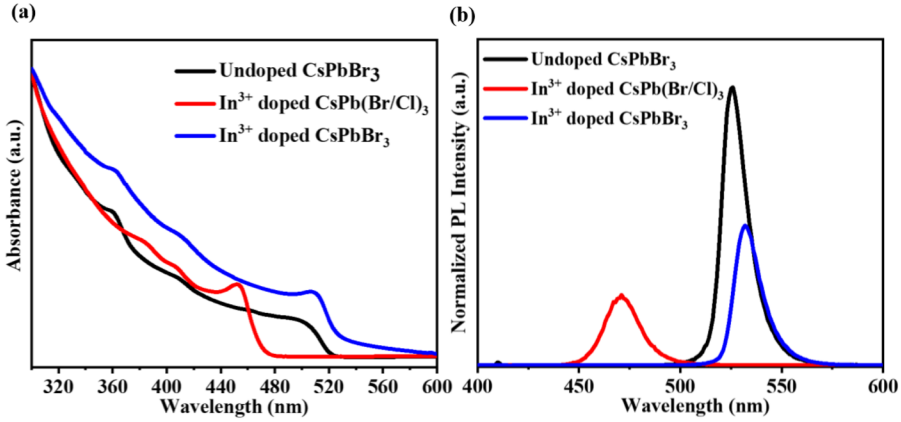

FIG. 5. (a) Absorption spectra of undoped $CsPbBr_3$ NCs, In^{3+} doped $CsPbBr_3$ NCs, and In^{3+} doped $CsPb(Br/Cl)_3$ NCs (In/Pb 0.5). (b) PL spectra of undoped $CsPbBr_3$ NCs, In^{3+} doped $CsPbBr_3$ NCs, and In^{3+} doped $CsPb(Br/Cl)_3$ NCs under excitation at 365 nm.

decreased when doping with In^{3+} and Cl^-. To explore the underlying mechanism of PL decay and describe the relaxation process in doped NCs, we use the following modified stretched exponential function to fit the decay curves:

$$I(t) = \exp\left(-\frac{t}{\tau} - a\left(\frac{t}{\tau}\right)^{\beta}\right), \tag{5}$$

where τ is the lifetime of the excited state of the NCs and the parameter a is proportional to the concentration of $InCl_3$. The stretch parameter β takes different values depending on the dimensionality of the medium ($0 < \beta \leq 1$). It has been demonstrated that different ranges of parameter β indicate different non-radiative transition processes.[36,37] For $\beta \leq 0.5$, the relaxation can be assigned to long-range resonance energy transfer between the donor and acceptor. For $\beta > 0.5$, the relaxation can be described in terms of the contact quenching mechanism (Förster energy transfer or electron transfer).[37] As shown in Table S3, all the samples were well fitted with parameter $\beta > 0.5$, indicating that the PL decay kinetics could be well described by contact quenching. The decreased lifetime indicates that non-radiative processes are enhanced by In^{3+} and Cl^- co-doping.[38–40]

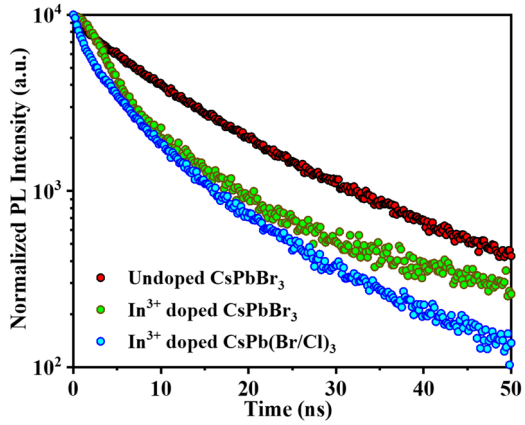

FIG. 6. TRPL profiles of undoped and doped NCs under laser excitation at 400 nm.

TABLE I. Calculated radiative (τ_r) and non-radiative (τ_{nr}) lifetimes for pristine and different doped $CsPbBr_3$ NCs.

Sample	PLQY (%)	τ_{obs} (ns)	τ_r (ns)	τ_{nr} (ns)
Undoped $CsPbBr_3$	78.86	16.06	20.37	75.90
In/Pb 0.5	20.58	9.29	45.14	11.70
In/Pb 2	10.36	4.19	40.44	4.67

To understand the impact of doping on the CT at the interface of the $CsPbBr_3$ NCs with molecular acceptors, we conducted PL and TRPL studies of undoped and doped NCs with tetracyanoethylene (TCNE), a strong electron acceptor, on the surface of the NCs. Figures 7(a) and 7(b) show the absorption and PL spectra of In^{3+} doped $CsPb(Br/Cl)_3$ NCs with compositing with TCNE. The PL quenching can be observed with the addition of TCNE, indicating a strong interaction between TCNE and NCs.[41] As shown in Figs. 7(b), S5(b), and S6(b), we observed quenching efficiencies of 79%, 83%, and 96% for the undoped $CsPbBr_3$ NCs, In^{3+} doped $CsPbBr_3$ NCs, and In^{3+} doped $CsPb(Br/Cl)_3$ NCs, respectively. Such PL quenching is usually attributed to electron transfer or non-radiative energy transfer (Förster mechanism).[36,42] The lack of spectral overlap between the absorption of TCNE and the emission of NCs rules out the possibility of Förster resonance energy transfer (FRET), as shown in Fig. S7.[11,43,44] Thus, photoinduced electron transfer from the photoexcited NCs to TCNE is the most likely mechanism involved in the PL quenching of the NCs. A slight red-shift in the absorption and PL emission peaks appears for In^{3+} doped $CsPb(Br/Cl)_3$ NCs when TCNE was added, which also indicates strong interaction between NCs and TCNE as well as the possible formation of a complex.[45] This is consistent with the proposed photoinduced electron transfer from NCs to TCNE.[15] On the contrary, the absorption spectra and PL peaks do not shift for the undoped and In^{3+} doped $CsPbBr_3$ NCs, which suggests a weaker interaction between these NCs and TCNE [Figs. S5(a), S5(b), S6(a), and S6(b)].[46]

To investigate in more detail the interactions between $CsPbBr_3$ NCs and TCNE, we performed the PL decay lifetime measurement for undoped and In^{3+} doped $CsPb(Br/Cl)_3$ NCs in the presence of

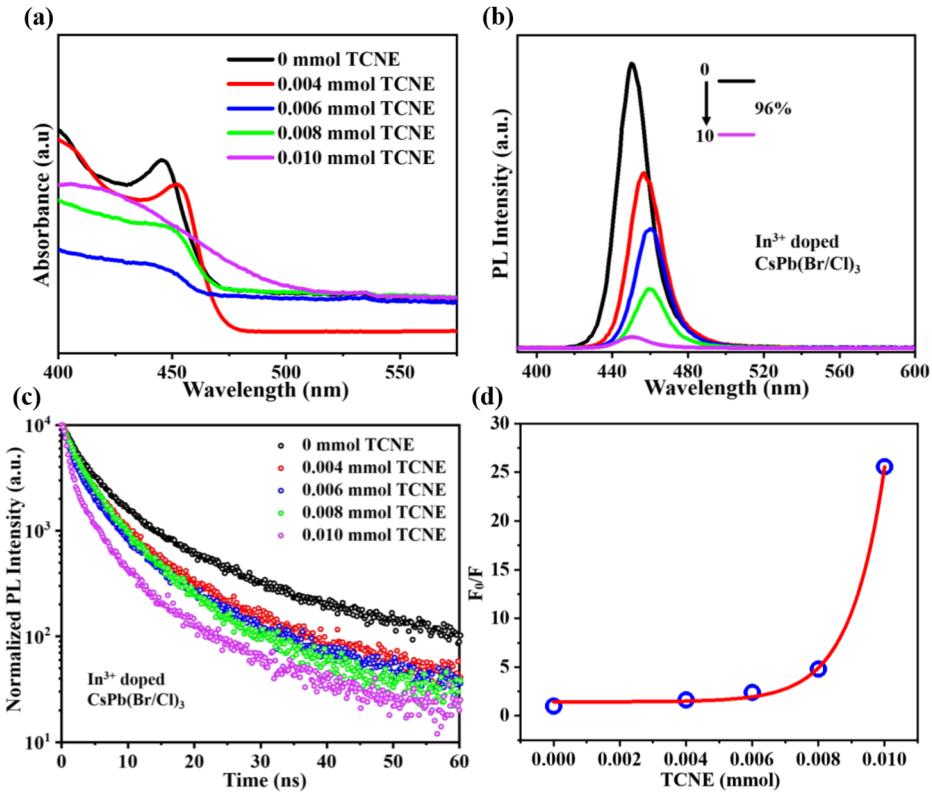

FIG. 7. (a) Absorption spectra and (b) the PL spectra of In^{3+} doped $CsPb(Br/Cl)_3$ NCs (In/Pb 0.5) in toluene upon successive addition of TCNE. (c) The PL lifetime of In^{3+} doped $CsPb(Br/Cl)_3$ NCs with TCNE was measured after laser excitation at 400 nm. (d) Stern–Volmer plot of PL quenching of In^{3+} doped $CsPb(Br/Cl)_3$ NCs.

TCNE. As shown in Figs. 7(c) and S6(c), the PL decay profiles are fitted with a biexponential function and the corresponding parameters are listed in Tables S4 and S5. The fast and slow decay components are attributed to charge carrier trapping and excitonic recombination, respectively.[47] We also fitted the PL decay curves using the stretched exponential function to explore the non-radiative transition between NCs and TCNE. The corresponding parameters are listed in Tables S6 and S7. The lifetime is much shorter for In^{3+} doped $CsPb(Br/Cl)_3$ NCs, indicating faster non-radiative processes (e.g., electron transfer) between NCs and TCNE.[38–40]

To further confirm the interaction between the NCs and TCNE, we compared the XPS results for In^{3+} doped $CsPb(Br/Cl)_3$ NCs before and after TCNE addition. As shown in Figs. S8(a)–S8(d), the Pb 4f and Br 3d peaks remain the same, while the In 3d and Cl 2p peaks shift to higher binding energy following TCNE addition, indicating the enhancement interaction between TCNE with In^{3+} and Cl^- of NCs.[48]

In order to understand the transfer mechanism of photoinduced electrons, we analyzed the PL quenching data using the Stern–Volmer equation. In this case, the Stern–Volmer equation followed the formula

$$\frac{F_0}{F} = (1 + K_D[Q])(1 + K_S[Q]), \tag{6}$$

where F and F_0 are the PL intensities with and without TCNE, respectively, K_D and K_S are the dynamic and static quenching constants, respectively, and [Q] is the concentrations of TCNE. This modified formula of the Stern–Volmer equation is the second order function of [Q] when both static quenching and dynamic quenching occur.[11] We estimated the dynamic and the static quenching constants at 0.10×10^3 and 0.83×10^3 M^{-1} for In^{3+} doped NCs and 0.11×10^3 and 0.79×10^3 M^{-1} for undoped NCs, respectively. As shown in Figs. 7(d) and S6(d), both undoped and doped NCs exhibit non-linear Stern–Volmer plots, which indicates that the PL quenching is controlled by the dynamic and static quenching mechanism.[49–51]

To investigate the impact of In^{3+} and Cl^- doping on the band structure of $CsPbBr_3$ NCs, we conducted ultraviolet photoemission spectroscopy (UPS) measurement to explore the change of valence band maximum (VBM) and Fermi level with respect to the vacuum level after doping [Figs. S9(a)–S9(c)]. The VBM of undoped $CsPbBr_3$ NCs, In^{3+} doped $CsPbBr_3$ NCs, and In^{3+} doped $CsPb(Br/Cl)_3$ NCs based on the UPS results was calculated to be −5.7, −5.1, and −5.2 eV, respectively. Meanwhile, we found that the Fermi level shifts upward from −4.2 to −3.5 eV after In^{3+} and Cl^- co-doping compared with undoped NCs. The VBM of $CsPbBr_3$ is known to consist of a mixture of nonbonding orbitals of *s*-type Pb orbitals and *p*-type Br orbitals, while the conduction band minimum (CBM) of $CsPbBr_3$ is composed of Pb 6p and Br 4s orbitals.[52] We resolved the broad peak in the UPS spectra corresponding to the Br 4p, Pb 6s, and Pb 6p orbital mixture, which is consistent with previous reports [Figs. S9(d)–S9(f)].[27,53,54]

The process of CT between NCs and TCNE is illustrated schematically in Fig. 8, along with related energy levels combining

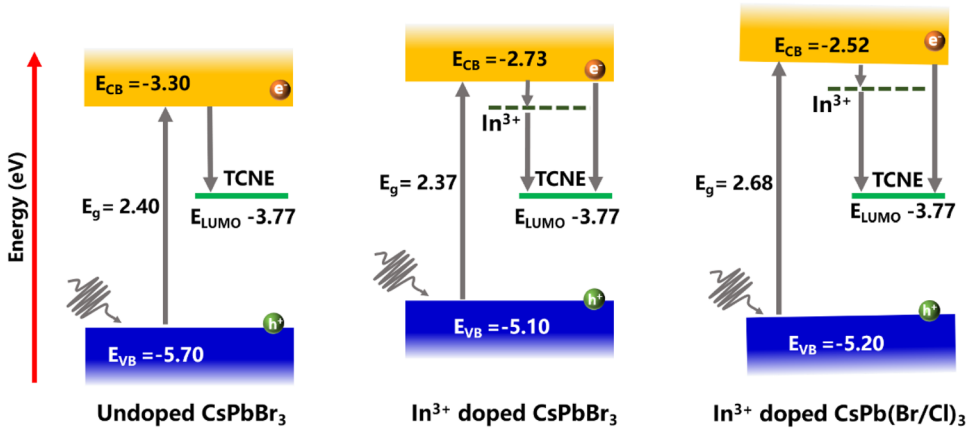

FIG. 8. Schematic illustration of the bandgap offset of undoped and In^{3+} and Cl^- co-doped $CsPbBr_3$ NCs with respect to the LUMO of TCNE (based on values reported in Refs. 15 and 27).

the VB positions and the optical bandgaps E_{opt} (CBM = VBM + E_{opt}). Based on the UPS spectra and literature, the valence band (VB) edge of the undoped NCs is −5.7 eV and LUMO values is −3.77 eV for TCNE vs vacuum.[15,27] According to Marcus theory, the rate constant of electron transfer (k_{et}) between the donor (A) and acceptor (B) pair can be described as the following equations:

$$k_{et} = \frac{2\pi}{\hbar}|H_{AB}|^2 \frac{1}{\sqrt{4\pi\lambda k_B T}} \exp\left(-\frac{(\lambda + \Delta G^0)^2}{4\lambda k_B T}\right), \quad (7)$$

where H_{AB} is the electronic coupling between the initial and final states, λ is the reorganization energy, ΔG^0 is the total Gibbs free energy change of the electron transfer reaction, k_B is Boltzmann's constant, and T is the temperature.[55] In this case, ΔG^0 is the energy difference between the bottom of the conduction band (CB) of the NCs and the LUMO levels of TCNE. After In^{3+} doping, the VB and CB edges of the NCs are shifted upward and the dopant energy level is introduced near the CB edge.[27] We assume that the reorganization energy and the overlap of the electronic wave functions of NCs and TCNE do not change after doping. Therefore, the enhanced k_{et} with In^{3+}-doped NCs can be attributed to increased ΔG^0.[15,48,56] There are two routes for the photogenerated electrons to transfer from In^{3+} doped NCs and In^{3+} doped $CsPb(Br/Cl)_3$ NCs to TCNE. The first is direct transfer from the CB of the NCs to the LUMO of TCNE. For the In^{3+} doped $CsPb(Br/Cl)_3$ NCs, the energy difference between the CB edge of the NCs and the LUMO levels of TCNE is even higher than that of In^{3+} doped $CsPbBr_3$ NCs due to Cl^- replacing Br^-, which further accelerates the electron transfer process, as illustrated in Fig. 8.[49,57] Therefore, according to Marcus theory, faster CT is expected for the In^{3+} doped $CsPb(Br/Cl)_3$ NCs than that of undoped and In^{3+}-doped NCs. Another possible route for photogenerated electrons to transfer to the LUMO of TCNE is through the In^{3+} dopant energy level. The dopant energy level may facilitate the electron transfer by reducing other non-radiative trapping processes or serving as a long-lived intermediate state to first accept the photoinduced electrons from the CB and then transfer to TCNE. This could also explain the enhanced electron transfer from the doped $CsPbBr_3$ NCs to TCNE.

IV. CONCLUSION

In summary, we have demonstrated an In^{3+} and Cl^- co-doping strategy to partially replace Pb^{2+} and Br^- in the matrix lattice of $CsPbBr_3$ through a ligand-assisted precipitation method at room temperature. The In^{3+} doped $CsPb(Br/Cl)_3$ NCs show the distinct PL quenching and shorter lifetimes. Mixed halide and metal ion doping promotes the carrier separation efficiency and CT from $CsPbBr_3$ NCs to molecular acceptors. The results demonstrate that the interfacial CT can be tuned and facilitated by In^{3+} and Cl^- co-doping, leading to the improvement of electron transfer efficiency, which is benefit to the progress of the interface photocatalytic reaction.

SUPPLEMENTARY MATERIAL

See the supplementary material for additional TEM and characterization data.

ACKNOWLEDGMENTS

This work was supported by the National Natural Science Foundation of China (Grant No. 21965003), the Opening Project of Guangxi Key Laboratory of Marine Natural Products and Combinatorial Biosynthesis Chemistry (Grant No. GXMNPC2020003), and the Guangxi Natural Science Foundation (Grant No. 2017GXNSFGA198005). J.Z.Z. acknowledges the U.S. NSF (Grant No. CHE-1904547) for financial support.

AUTHOR DECLARATIONS

Conflict of Interest

The authors have no conflicts to disclose.

DATA AVAILABILITY

The data that support the findings of this study are available within the article and its supplementary material.

REFERENCES

[1] L. Protesescu, S. Yakunin, M. I. Bodnarchuk, F. Krieg, R. Caputo, C. H. Hendon, R. X. Yang, A. Walsh, and M. V. Kovalenko, Nano Lett. **15**, 3692 (2015).
[2] J. Liang, D. Chen, X. Yao, K. Zhang, F. Qu, L. Qin, Y. Huang, and J. Li, Small **16**, 1903398 (2020).
[3] T. Qiao and D. H. Son, Acc. Chem. Res. **54**, 1399 (2021).
[4] S. S. H. Abir, S. K. Gupta, A. Ibrahim, B. B. Srivastava, and K. Lozano, Adv. Mater. Res. **2**, 2700 (2021).
[5] P. Chen, W. J. Ong, Z. Shi, X. Zhao, and N. Li, Adv. Funct. Mater. **30**, 1909667 (2020).
[6] R. X. Yang, J. M. Skelton, E. L. Da Silva, J. M. Frost, and A. Walsh, J. Chem. Phys. **152**, 024703 (2020).
[7] S.-H. Guo, J. Zhou, X. Zhao, C.-Y. Sun, S.-Q. You, X.-L. Wang, and Z.-M. Su, J. Catal. **369**, 201 (2019).
[8] W.-G. Li, X.-D. Wang, J.-F. Liao, Z.-F. Wei, Y.-F. Xu, H.-Y. Chen, and D.-B. Kuang, J. Mater. Chem. C **7**, 5670 (2019).
[9] Z. Guan, Y. Wu, P. Wang, Q. Zhang, Z. Wang, Z. Zheng, Y. Liu, Y. Dai, M.-H. Whangbo, and B. Huang, Appl. Catal., B **245**, 522 (2019).
[10] Y. Wu, P. Wang, Z. Guan, J. Liu, Z. Wang, Z. Zheng, S. Jin, Y. Dai, M.-H. Whangbo, and B. Huang, ACS Catal. **8**, 10349 (2018).
[11] E. Rathore, K. Maji, D. Rao, B. Saha, and K. Biswas, J. Phys. Chem. Lett. **11**, 8002 (2020).
[12] J. Zhang, C. Xie, G. Li, P. Dai, L. Yang, R. Liu, and B. Pan, J. Chem. Phys. **151**, 134104 (2019).
[13] G. H. Ahmed, J. Yin, O. M. Bakr, and O. F. Mohammed, J. Chem. Phys. **152**, 020902 (2020).
[14] B. Ke, R. Zeng, Z. Zhao, Q. Wei, X. Xue, K. Bai, C. Cai, W. Zhou, Z. Xia, and B. Zou, J. Phys. Chem. Lett. **11**, 340 (2020).
[15] R. Begum, M. R. Parida, A. L. Abdelhady, B. Murali, N. M. Alyami, G. H. Ahmed, M. N. Hedhili, O. M. Bakr, and O. F. Mohammed, J. Am. Chem. Soc. **139**, 731 (2017).
[16] W. Shi, T. Cai, Z. Wang, and O. Chen, J. Chem. Phys. **153**, 141101 (2020).
[17] Z.-K. Wang, M. Li, Y.-G. Yang, Y. Hu, H. Ma, X.-Y. Gao, and L.-S. Liao, Adv. Mater. **28**, 6695 (2016).
[18] Z. Han, C. Tang, J. Wang, L. Li, and C. Li, J. Catal. **394**, 236 (2021).
[19] Z. Li, Z. Wu, S. Zhang, J. Shen, W. Feng, Y. Du, L. Wan, and S. Zhang, Dalton Trans. **47**, 8110 (2018).
[20] H. Li, Y. Xia, Z. Liang, G. Ba, and W. Hou, ACS Appl. Energy Mater. **3**, 377 (2020).
[21] W. Chu, Q. Zheng, O. V. Prezhdo, J. Zhao, and W. A. Saidi, Sci. Adv. **6**, eaaw7453 (2020).
[22] J. Kang, J. Li, and S.-H. Wei, Appl. Phys. Rev. **8**, 031302 (2021).
[23] K. N. Fu, Y. P. He, B. Zhang, X. W. Gao, and G. Z. Zou, J. Electroanal. Chem. **858**, 113835 (2020).
[24] F. Mcgrath, U. V. Ghorpade, and K. M. Ryan, J. Chem. Phys. **152**, 174702 (2020).
[25] C. Liu, W. Li, H. Li, H. Wang, C. Zhang, Y. Yang, X. Gao, Q. Xue, H.-L. Yip, J. Fan, R. E. I. Schropp, and Y. Mai, Adv. Energy Mater. **9**, 1803572 (2019).
[26] F. Alam, K. D. Wegner, S. Pouget, L. Amidani, K. Kvashnina, D. Aldakov, and P. Reiss, J. Chem. Phys. **151**, 231101 (2019).
[27] Arramel, A. Xie, X. Yin, C. S. Tang, M. H. Mahyuddin, C. Hettiarachchi, M. F. Sahdan, K. Yoshizawa, C. Dang, M. D. Birowosuto, A. T. S. Wee, and A. Rusydi, ACS Appl. Energy Mater. **3**, 7500 (2020).
[28] A. Shapiro, M. W. Heindl, F. Horani, M.-H. Dahan, J. Tang, Y. Amouyal, and E. Lifshitz, J. Phys. Chem. C **123**, 24979 (2019).
[29] J.-S. Yao, J. Ge, B.-N. Han, K.-H. Wang, H.-B. Yao, H.-L. Yu, J.-H. Li, B.-S. Zhu, J.-Z. Song, C. Chen, Q. Zhang, H.-B. Zeng, Y. Luo, and S.-H. Yu, J. Am. Chem. Soc. **140**, 3626 (2018).
[30] J. C. Brauer, D. Tsokkou, S. Sanchez, N. Droseros, B. Roose, E. Mosconi, X. Hua, M. Stolterfoht, D. Neher, U. Steiner, F. De Angelis, A. Abate, and N. Banerji, J. Chem. Phys. **152**, 104703 (2020).
[31] R. A. Scheidt and P. V. Kamat, J. Chem. Phys. **151**, 134703 (2019).
[32] D. Ricciarelli, D. Meggiolaro, P. Belanzoni, A. A. Alothman, E. Mosconi, and F. De Angelis, ACS Energy Lett. **6**, 1869 (2021).
[33] S. B. Naghadeh, B. Luo, Y.-C. Pu, Z. Schwartz, W. R. Hollingsworth, S. A. Lindley, A. S. Brewer, A. L. Ayzner, and J. Z. Zhang, J. Phys. Chem. C **123**, 4610 (2019).
[34] Z. Zhang and B. Saparov, Appl. Phys. Lett. **119**, 030502 (2021).
[35] P. Maji, A. Ray, P. Sadhukhan, S. Chatterjee, and S. Das, J. Appl. Phys. **124**, 124102 (2018).
[36] E. N. Bodunov and A. L. Simões Gamboa, Semiconductors **52**, 587 (2018).
[37] E. N. Bodunov, Y. A. Antonov, and A. L. Simoes Gamboa, J. Chem. Phys. **146**, 114102 (2017).
[38] E. N. Bodunov, V. V. Danilov, A. S. Panfutova, and A. L. Simões Gamboa, Ann. Phys. **528**, 272 (2016).
[39] O. Stroyuk, A. Raevskaya, F. Spranger, N. Gaponik, and D. R. T. Zahn, ChemPhysChem **20**, 1640 (2019).
[40] M. Li, S. R. Valandro, R. He, Y. Zhao, P. Yang, and K. S. Schanze, J. Phys. Chem. C **125**, 14778 (2021).
[41] X. Zhu, J. Chem. Phys. **153**, 030401 (2020).
[42] Y. Kanemitsu, J. Chem. Phys. **151**, 170902 (2019).
[43] K. R. Pradeep and R. Viswanatha, APL Mater. **8**, 020901 (2020).
[44] H. Leng, J. Loy, V. Amin, E. A. Weiss, and M. Pelton, ACS Energy Lett. **1**, 9 (2016).
[45] Y. Wang, K. Chen, H. Hao, G. Yu, B. Zeng, H. Wang, F. Zhang, L. Wu, J. Li, S. Xiao, J. He, Y. Zhang, and H. Zhang, Nanoscale **11**, 2637 (2019).
[46] S. Dey, H. Cohen, I. Pinkas, H. Lin, M. Kazes, and D. Oron, J. Chem. Phys. **151**, 174704 (2019).
[47] T. J. Miao and J. Tang, J. Chem. Phys. **152**, 194201 (2020).
[48] G. H. Ahmed, J. Liu, M. R. Parida, B. Murali, R. Bose, N. M. Alyami, M. N. Hedhili, W. Peng, J. Pan, T. M. D. Besong, O. M. Bakr, and O. F. Mohammed, J. Phys. Chem. Lett. **7**, 3913 (2016).
[49] D. Genovese, M. Cingolani, E. Rampazzo, L. Prodi, and N. Zaccheroni, Chem. Soc. Rev. **50**, 8414 (2021).
[50] G. Hollett, D. S. Roberts, M. Sewell, E. Wensley, J. Wagner, W. Murray, A. Krotz, B. Toth, V. Vijayakumar, and M. J. Sailor, J. Phys. Chem. C **123**, 17976 (2019).
[51] J.-F. Liao, W.-Q. Wu, Y. Jiang, J.-X. Zhong, L. Wang, and D.-B. Kuang, Chem. Soc. Rev. **49**, 354 (2020).
[52] G. Xiao, Y. Cao, G. Qi, L. Wang, C. Liu, Z. Ma, X. Yang, Y. Sui, W. Zheng, and B. Zou, J. Am. Chem. Soc. **139**, 10087 (2017).
[53] A. R. Kirmani, A. E. Mansour, M. I. Saidaminov, X. Cui, D. Shi, A. Alofi, Y. B. Losovyj, G. Gurung, T. R. Paudel, A. J. Yost, P. A. Dowben, E. Y. Tsymbal, A. Amassian, and K. Katsiev, Appl. Phys. Lett. **113**, 022101 (2018).
[54] J. Endres, D. A. Egger, M. Kulbak, R. A. Kerner, L. Zhao, S. H. Silver, G. Hodes, B. P. Rand, D. Cahen, L. Kronik, and A. Kahn, J. Phys. Chem. Lett. **7**, 2722 (2016).
[55] A. Brumberg, B. T. Diroll, G. Nedelcu, M. E. Sykes, Y. Liu, S. M. Harvey, M. R. Wasielewski, M. V. Kovalenko, and R. D. Schaller, Nano Lett. **18**, 4771 (2018).
[56] Y.-C. Pu, H. Ma, N. Sajben, G. Xia, J. Zhang, Y. Li, and J. Z. Zhang, ACS Appl. Energy Mater. **1**, 2907 (2018).
[57] V. K. Ravi, G. B. Markad, and A. Nag, ACS Energy Lett. **1**, 665 (2016).